Acetylene pyrolysis applied to vacuum carburizing: experimental studies and numerical simulation of precursor decomposition

W. Dal'Maz Silva[a,b,*], J. Dulcy[a], P. Lamesle[b], T. Belmonte[a,**]

[a] *Institut Jean Lamour, Parc de Saurupt, Nancy 54011, France*
[b] *Institut de Recherche Technologique M2P, Metz 57070, France*

Abstract

Acetylene pyrolysis has extensively been studied in the last decades due to the large amount of applications of this precursor in several industrial branches. These include deposition processes, vapor infiltration and carburizing of steel among others. A detailed mechanism of hydrocarbon decomposition compiled by Norinaga et al. [1] and validated for some species as precursors, including acetylene pyrolysis, is studied. Satisfactory results are obtained for the main reaction by-products of C_2H_2 decomposition around 1173 K simulated using this mechanism comprised by 241 species and 902 reactions. A modified version of the directed relational graph (DRG) approach by Lu and Law [2] is used for simplification of this mechanism and results are compared to experimental results. Additionally, chemical graph structure is studied in detail, providing an insightful view of species coupling.

Keywords: acetylene, directed relational graph, mechanism simplification, gas chromatography

1. Introduction

Vacuum steel carburizing is a case hardening treatment of mechanical components intended for surface load bearing applications such as power transmission parts and gears. Regarding classical carburizing [3, 4], the main difference of the low pressure process is the absence of the oxide layer formed in the partially oxidizing CO − H_2 atmosphere. The process profits from low molecular weight hydrocarbons – such as CH_4, C_2H_2, C_2H_4 and C_3H_8 – as carbon sources and it has been studied from both metallurgical [5–11] and kinetics [12–15] standpoints. Although the literature is limited in the description of process kinetics specifically devoted to carburizing, much has been published about its common precursors decomposition [1, 15–32] with respect to their sooting characteristics and reaction pathways to undesired species such as polycyclic aromatic hydrocarbons (PAH).

The present work aims at investigating the decomposition of C_2H_2 under conditions relevant to vacuum steel carburizing. At first, acetylene decomposition is studied diluted in nitrogen in a vertical tubular flow reactor. These experiments were carried out at atmospheric pressure under partial pressures equivalent to those employed in steel treatment (around 20 hPa) but with much longer residence times (in the order of 100 s). Reduced pressure studies were carried in an horizontal tubular flow reactor with the same partial pressure range but residence times are reduced to the order of 1 s. Results are confronted to available literature data and compared to both global models [14, 27, 33] and detailed chemical kinetics [1]. Low pressure results were represented by a plug flow reactor (PFR) given the high flow speeds resulting in an relatively high Péclet number [34].

Numerical studies were performed with routines implemented with chemical kinetics library Cantera [35] and graph search algorithms from NetworkX [36]. In order to provide a simpler mechanism for future industrial process simulation, Norinaga et al. [1] mechanism is submitted to directed relational graph (DRG) simplification [2, 37–39]. Although the method has been criticized [40] and a more feature complete scheme exists such as CSP [41–43], it is of simple implementation and interpretation, it has already been employed for our purpose [44] and recently was used for automated mechanism simplification [45]. Furthermore, the graph approach allows for mechanism structure analysis [46].

*Corresponding author
**Principal corresponding author
Email addresses:
walter.dal-maz-silva@univ-lorraine.fr (W. Dal'Maz Silva), jacky.dulcy@univ-lorraine.fr (J. Dulcy), gregory.michel@irt-m2p.fr (G. Michel), thierry.belmonte@univ-lorraine.fr (T. Belmonte)

2. Materials and methods

2.1. Atmospheric pressure experimental setup

The vertical tubular flow reactor employed in the atmospheric pressure experiments has a diameter of 50 mm and total tube length of 60 cm. Gas injection is performed by a 2 mm-diameter tube with its extremity placed at 25 cm from the reactor top, leading to an equivalent length with restrained gas circulation. Heated zone is 20 cm long and starts 30 cm below the reactor top. Temperature set-point is found to be homogeneous in a length of 10 cm centered in the heated region. The lower part of the reactor is symmetric with the previously described upper part. Reactor outlet is kept at atmospheric pressure and flue gas is partially conducted to a Carlo Erba GC6000 Vega Series 2 gas chromatograph (GC) equipped with both a flame-ionization (FID) and a thermal-conductivity (TCD) detectors for gas characterization.

Atmosphere composition was fixed to $N_2 - 0.02\,C_2H_2$ (given in mole fractions), leading to a partial pressure of acetylene around 20 hPa. Heated zone temperature was set between 873 K to 1223 K and total volume flow rates of 500 $cm^3\,min^{-1}$ and 1000 $cm^3\,min^{-1}$ were employed. Gas phase hydrocarbons up to C_2 where identified by FID-GC and H_2 by TCD-GC. Probability density functions for different flow rates were measured by the tracer pulse method [34] with the heated zone of the vertical tubular reactor set to 1173 K. Methane was employed as tracer gas given its reasonable stability at operating temperature in the absence of oxygen (no C_2 reaction by-products are observed under the experimental conditions). Injection volume for the pulse was 10 mL (approximately 2.5% of the heated zone volume). These measurements are intended to suit the needs of a global decomposition order analysis at long residence times ($\tau_{eff} > 50$ s).

2.2. Reduced pressure experimental setup

Low pressure studies were carried in a horizontal quartz tubular flow reactor of 80 cm in length and diameter of 28 mm. Gas injection is performed 20 cm before the arrival to heated zone in order to ensure a fully established flow in this region. Temperature is controlled over a length of 40 cm, the remaining of the tube leading to the outlet and gas chromatography system. Figure A.7 presents the actual wall temperature profile measured with a type-K thermocouple along the reactor axis. Gas phase pyrolysis products were analyzed using a Perkins Elmer GC system equipped with a TCD and a gas compression system adapted the GC for low pressure sampling. Separated species comprise C_2H_2, CH_4, C_2H_4, C_2H_6, CO and N_2. Assuming that N_2 does not take part in the pyrolysis mechanism other than a third-body, its outlet mole fraction can be used to estimate actual residence time τ_{eff} and changes in volume flow rate due to average molar mass change.

Pyrolysis was studied with an atmosphere composed of $N_2 - 0.36\,C_2H_2$ (given in mole fractions) in the temperature range of 773 K to 1273 K and total pressures of 30 hPa to 100 hPa. Reference atmospheric volume flow rates were set in the range from 222 $cm^3\,s^{-1}$ to 378 $cm^3\,s^{-1}$. These conditions lead to acetylene partial pressures in the range of 11 hPa to 36 hPa.

2.3. Computational methods and tools

Global order analysis coupled to residence time distribution (RTD) was carried for atmospheric pressure decomposition of C_2H_2. These estimations considered decomposition to take place in the homogeneous temperature region of the reactor. It is proposed that the RTD of this region can be approximated by the peak and decay tail of the approximately tubular flow reactor measured distribution (the delay before the peak can be attributed to a plug-like behavior after the heated zone) as shown in Fig. **??**. Acetylene conversion was computed with aid of RTD data by assuming a maximum mixedness model originally attributed to Zwietering [33].

Reduced pressure results were represented by a plug-flow reactor (PFR) model implemented with the Python interface of chemical kinetics library Cantera [35]. This model assumption is reasonable given the Péclet number $Pe \gg 1$ which can be computed for the system[1]. Tube length is divided in small lengths δ, each being represented by a perfect stirred reactor (PSR) model. The first reactor is fed with the inlet gas and its steady-state solution is then employed to feed the next reactor in the network and so on until the whole length is covered. Discretization length δ was reduced until the relative difference between consecutive outlet solutions for selected species (C_2H_2, H_2, C_2H_4, C_4H_4 and C_6H_6) fall below 10^{-6}.

A detailed mechanism assembled by Norinaga et al. [1] was used for the first set of simulations. Inlet N_2 was assumed to be free from contaminants, while C_2H_2 composition took into account recommended values [28] of impurities, as given in Tab. 1. In order to represent actual temperature profiles, convective heat transfer was

[1] See generated simplified mechanism file. The computation of Péclet number $Pe \approx 300$ considered the average diffusivity – provided by Cantera [35] using Lennard-Jonnes model – of all species at 1173 K and 5000 Pa.

added to the simulations by considering a constant local wall temperature (Nusselt number Nu = 3.66) and global heat transfer coefficient $\bar{U} = k\,\mathrm{Nu}\,\delta^{-1}$. Gas thermal conductivity was computed using a mixing model with Cantera [35] built-in functions.

Table 1: Inlet acetylene gas composition given in mole fractions adopted for simulations. Nitrogen carrier is assumed free of impurities and its proportion in the mixture is identical to the experimental conditions.

C_2H_2	CH_3COCH_3	CH_4
0.980	0.018	0.002

For mechanism simplification, Lu and Law [2] method was implemented in Python with NetworkX [36] graph library. For the computation of relative species interaction terms of the directed relational graph (DRG), Cantera [35] was again employed. By using a fixed atmosphere composition, isothermal PSR integration were carried out at different pressures to obtain a sampling space of solutions for relative interaction parameters computation. Under all circumstances above, kinetics and state equations were integrated with Sundials [47] ordinary differential equation solver CVode.

In order to verify the accuracy and proper functioning of the simplified mechanism here proposed, the system was simulated in 2-D using OpenFOAM [48] on its version 5.0 with solver *reactingFoam*. System pressure was set to 5000 Pa and heated zone temperature to 1173 K. Inlet velocity was set to match the flow of $N_2 - 0.36\,C_2H_2$ at 298 K with a flow rate of $222\,\mathrm{cm^3\,min^{-1}}$.

3. Results and discussion

3.1. Atmospheric pressure decomposition

The resulting decomposition of diluted hydrocarbons at atmospheric pressure as described in Section 2.1 are presented in Figures 1 and 2. Acetylene (C_2H_2) decomposition is depicted in Fig. 1 showing that at 873 K, the lowest temperature employed in the study of atmospheric pressure pyrolysis, the compound remains stable during the experiment time-scale and thus measurements were carried only for low total flow rate ($500\,\mathrm{cm^3\,min^{-1}}$). A temperature increase of just 50 K with respect to this reference stability point is enough to start decomposition, which is observed to increase rapidly with temperature. Since experiments were carried under same room temperature flow rate but at different temperatures, no direct kinetic exploitation can be done to check measurement accuracy. One can start this verification by assuming acetylene pyrolysis follows a second order global path, as well established in the literature. Assuming that the system behaves as a stirred reactor with small volume change due to decomposition of acetylene in the mixture – thus inlet flow rate $\dot{Q}_{in}$ equals outlet flow rate $\dot{Q}_{out}$, or simply $\dot{Q}$ – and a quick approach of thermal steady state, an Arrhenius rate constant $k(T)$ can be adjusted to experimental data by optimizing the mole balance Eq. 1 below

$$\dot{Q}\,C^0_{Ac} - \dot{Q}\,C^\infty_{Ac} - 2\,k(T)\,C^\infty_{Ac} = 0 \qquad (1)$$

where inlet C_2H_2 composition is given by C^0_{Ac} and its measured steady-state counterpart by C^∞_{Ac}. It must be emphasized that flow rate $\dot{Q}$ needs to be corrected to take into account the expansion from room to operating temperature[2]. This procedure provides a rate constant given by Eq. 2 in units of $\mathrm{cm^3\,mol^{-1}\,s^{-1}}$. Both rate pre-exponential factor and activation energy in this constant match the order of magnitude of those for reactions $C_2H_2 + C_2H_2 \rightleftharpoons C_4H_4$ and $C_2H_2 + C_2H_2 \rightleftharpoons C_4H_2 + H_2$ as reported by Norinaga et al. [1], and thus the measurements are validated. Table 2 presents the measured outlet acetylene mole fractions from Fig. 1 alongside the values computed by integrating a second order process of pyrolysis with the aforementioned assumptions. Error is expected to be greater for $1000\,\mathrm{cm^3\,min^{-1}}$ since it is possible that the flow rate is high enough so that gas does not attain homogeneous setup temperature.

$$k(T) = 1.36 \times 10^{11} \exp\left[\frac{-179,180}{RT}\right] \qquad (2)$$

In the range of temperatures from 873 K to 973 K small quantities of the measured by-products (H_2, CH_4 and C_2H_4) are detected, although the conversion of C_2H_2 is around 30%. This could possibly be explained by the well known starting reaction of acetylene pyrolysis under the considered conditions, $C_2H_2 + C_2H_2 \rightleftharpoons C_4H_4$. The parallel process explaining the formation of the small quantities of H_2 may be linked to the reaction $C_2H_2 + C_2H_2 \rightleftharpoons C_4H_2 + H_2$. Regarding the numerical analysis of the pyrolysis process, it is expected that the maximum stiffness of the rate equations for the studied conditions be found somewhere between 973 K and 1023 K once it represents a rapid increase in pyrolysis advance.

Another important feature is the temperature for which CH_4 and C_2H_4 reach an apparent maximum in

[2]Thus, setup flow rate has to be multiplied by the ratio of reactor and room temperatures.

Table 2: Acetylene decomposition conditions.

Inlet composition	**Pressure** (hPa)	**Total flow rate** ($cm^3\,min^{-1}$)	**Temperature** (K)	**C_2H_2 mole fraction** measured	computed
N_2 – 0.02 C_2H_2	1000	500	873	0.020768	0.019565
			923	0.017902	0.017578
			973	0.014093	0.014423
			1023	0.010813	0.010981
			1073	0.007953	0.008045
			1123	0.005995	0.005836
			1173	0.004247	0.004259
			1223	0.003131	0.003151
		1000	1023	0.013880	0.013431
			1073	0.010945	0.010310
			1123	0.008762	0.007714
			1173	0.006963	0.005744
			1223	0.005377	0.004307
N_2 – 0.36 C_2H_2	30	222	1123		
			1173		
			1223		
	50	222	773		
			873		
			973		
			1023		
			1073		
			1123		
			1173		
			1273		
	100	222	1173		
			1223		
			1273		
		378	1023		
			1123		

Figure 2. While at lower temperatures the main reaction pathways of acetylene decomposition lead to polycyclic aromatic hydrocarbons (PAH), above 1173 K sooting also becomes important and hydrogen release with consumption of low molecular weight species are accelerated. For applications such as vacuum steel carburizing this temperature represents a technological limit.

Above 1023 K, Figure 1 provides measurements for both 500 $cm^3\,min^{-1}$ and 1000 $cm^3\,min^{-1}$. The main apparent effect of the increased flow rate is to *delay* acetylene decomposition without any important change in reaction pathways since curves follow approximately parallel. This is due to the smaller residence time imposed by the higher flow rate, roughly half of the one at 500 $cm^3\,min^{-1}$, as depicted in Figure **??**. As expected, these curves show a laminar tubular flow reactor since globally Reynolds number Re < 1 with the given operating conditions.

Mole balance analyses of the atoms composing the measured species are presented in Figure 3 and confirm ...

3.2. Low pressure decomposition

3.3. Mechanism simplification

3.4. Numerical simulation

4. Conclusion

Acknowledgments

The authors are grateful to CNRS and IRT M2P for the financial support. We would also like to acknowledge the companies Safran, PSA Peugeot Citroën, Faurecia, ECM Technologies, Ascometal, Air Liquide, Airbus Helicopters, Arcelor Mittal, UTC Aerospace Systems and Poclain Hydraulics for the supply of raw materials and financial support through IRT M2P.

Appendix A. Temperature profiles

Appendix B. Simplified mechanism

References

References

[1] K. Norinaga, O. Deutschmann, N. Saegusa, J. ichiro Hayashi, Analysis of pyrolysis products from light hydrocarbons and ki-

Table 3: Comparison between experimental and simulated (PFR model) acetylene output fractions.

Table 4: Initial conditions for PSR solution sampling of solution space state for mechanism simplification.

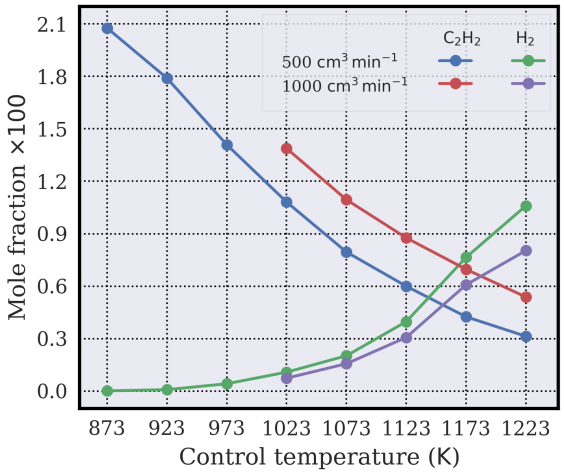

Figure 1: Measured mole fractions of C_2H_2 and H_2 at atmospheric pressure in terms of heated zone control temperature for different flow rates.

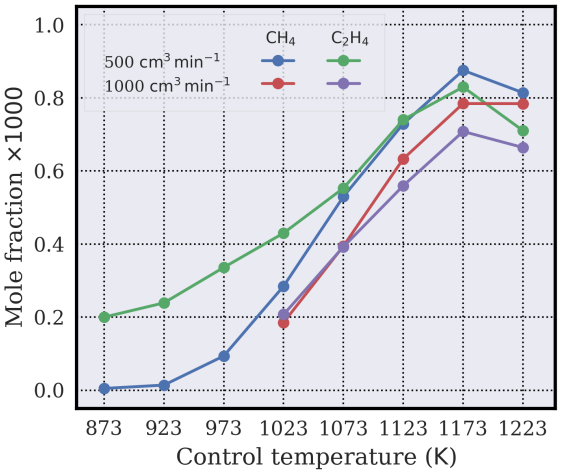

Figure 2: Measured mole fractions of CH_4 and C_2H_4 at atmospheric pressure in terms of heated zone control temperature for different flow rates.

netic modeling for growth of polycyclic aromatic hydrocarbons with detailed chemistry, Journal of Analytical and Applied Pyrolysis 86 (2009) 148 – 160. doi:doi:10.1016/j.jaap.2009.05.001.

[2] T. Lu, C. K. Law, A directed relation graph method for mechanism reduction, Proceedings of the Combustion Institute 30 (2005) 1333 – 1341. doi:doi:10.1016/j.proci.2004.08.145.

[3] J. Slycke, T. Ericsson, A study of reactions occurring during the carbonitriding process, Journal of Heat Treatment 2 (1981) 3–19. doi:doi:10.1007/BF02833069.

[4] J. Slycke, T. Ericsson, A study of reactions occurring during the carbonitriding process part ii, Journal of Heat Treatment 2 (1981) 97–112. doi:doi:10.1007/BF02833226.

[5] S. Tsuji, I. Ishigami, K. Yamanaka, Vacuum carburizing of low carbon steel with methane, Transactions of the Japan Institute of Metals 28 (1987) 48–56.

[6] L.-D. Liu, F.-S. Chen, The influences of alloy elements on the carburized layer in steels using vacuum carburization in an acetylene atmosphere, Materials Chemistry and Physics 82 (2003) 288–294. doi:doi:10.1016/S0254-0584(03)00239-6.

[7] P. Kula, R. Pietrasik, K. Dybowski, Vacuum carburizing–process optimization, Journal of Materials Processing Technology 164-165 (2005) 876–881. doi:doi:10.1016/j.jmatprotec.2005.02.145.

[8] P. Kula, Łukasz Kaczmarek, K. Dybowski, R. Pietrasik, M. Krasowski, Activation of carbon deposit in the process of vacuum carburizing with preliminary nitriding, Vacuum 87 (2013) 26 – 29. doi:doi:10.1016/j.vacuum.2012.06.018, including rapid communications, original articles and a special section with papers from the Proceedings of the Eleventh International Symposium on Sputtering and Plasma Processes (ISSP 2011) 6–8 July 2011, Kyoto, Japan.

[9] R. Gorockiewicz, A. Łapiński, Structure of the carbon layer deposited on the steel surface after low pressure carburizing, Vacuum 85 (2010) 429 – 433. doi:doi:10.1016/j.vacuum.2010.08.005.

[10] R. Gorockiewicz, The kinetics of low-pressure carburizing of low alloy steels, Vacuum 86 (2011) 448–451.

[11] M. Zajusz, K. Tkacz-Śmiech, M. Danielewski, Modeling of vacuum pulse carburizing of steel, Surface and Coatings Technology 258 (2014) 646 – 651. doi:doi:10.1016/j.surfcoat.2014.08.023.

[12] H. Iwata, Advanced acetylene vacuum carburizing, IHI Engineering review 38 (2005) 83–88.

[13] K. Yada, O. Watanabe, Reactive flow simulation of vacuum carburizing by acetylene gas, Computers and Fluids 79 (2013) 65–76.

[14] F. Graf, Pyrolyse- unf Aufkohlungsverhalten von C_2H_2 bei der Vakuumaufkohlung von Stahl, Ph.D. thesis, Universität Karlsruhe (TH), 2007.

[15] R. U. Khan, Vacumm Gas Carburizing - Fate of Hydrocarbons, Ph.D. thesis, Universität Karlsruhe (TH), 2008.

[16] W. Benzinger, A. Becker, K. Hüttinger, Chemistry and kinetics of chemical vapour deposition of pyrocarbon: I. fundamentals of kinetics and chemical reaction engineering, Carbon 34 (1996) 957 – 966. doi:doi:http://dx.doi.org/10.1016/0008-6223(96)00010-3.

[17] A. Becker, K. Hüttinger, Chemistry and kinetics of chemical vapor deposition of pyrocarbon: Ii pyrocarbon deposition from ethylene, acetylene and 1,3-butadiene in the low temperature regime, Carbon 36 (1998) 177 – 199. doi:doi:http://dx.doi.org/10.1016/S0008-6223(97)00175-9.

[18] A. Becker, K. Hüttinger, Chemistry and kinetics of chemical vapor deposition of pyrocarbon: Iii pyrocarbon deposition from propylene and benzene in the low temperature regime, Carbon 36 (1998) 201 – 211. doi:doi:http://dx.doi.org/10.1016/

Table B.5: Species to keep for the skeletal mechanism obtained for acetylene pyrolysis from the mechanism by Norinaga et al. [1].

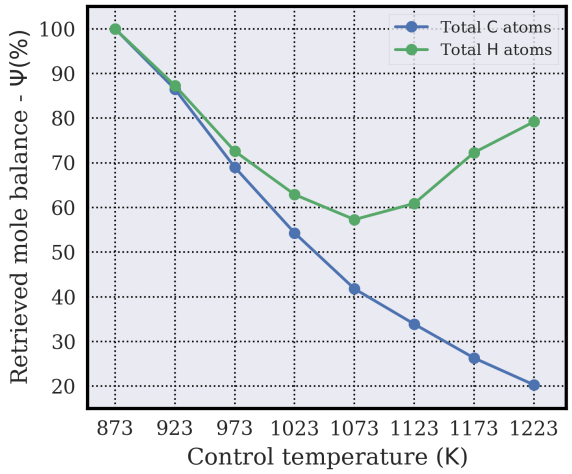

Figure 3: Retrieved percentage of carbon and hydrogen atoms at atmospheric pressure reactor outlet computed from species measurements presented in Figures 1 and 2 (flow rate of 500 cm^3 min^{-1}).

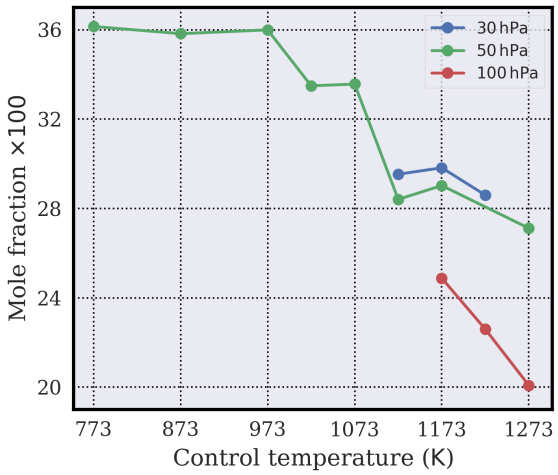

Figure 4: Measured mole fractions of C_2H_2 at different reduced pressures in terms of heated zone control temperature for a total inlet flow rate of 222 cm^3 min^{-1} of N_2 – 0.36 C_2H_2.

Figure 5: Number of residual species against simplification threshold factor η.

Figure 6: Comparison between full and simplified mechanisms of solution profiles along reactor axis for selected species.

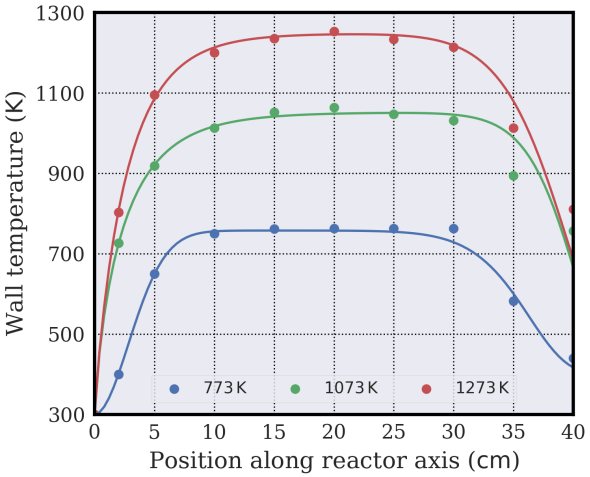

Figure A.7: Measured wall temperature profiles along horizontal reactor axis for selected temperatures. Adjusted curves are provided as lines while actual measurements are depicted as dots.

S0008-6223(97)00176-0.

[19] A. Becker, K. Hüttinger, Chemistry and kinetics of chemical vapor deposition of pyrocarbon: Iv pyrocarbon deposition from methane in the low temperature regime, Carbon 36 (1998) 213 – 224. doi:doi:http://dx.doi.org/10.1016/S0008-6223(97)00177-2.

[20] A. Becker, K. Hüttinger, Chemistry and kinetics of chemical vapor deposition of pyrocarbon: V influence of reactor volume/deposition surface area ratio, Carbon 36 (1998) 225 – 232. doi:doi:http://dx.doi.org/10.1016/S0008-6223(97)00178-4.

[21] I. Ziegler, R. Fournet, P.-M. Marquaire, Influence of surface on chemical kinetic of pyrocarbon deposition obtained by propane pyrolysis, Journal of Analytical and Applied Pyrolysis 73 (2005) 107 – 115. doi:doi:10.1016/j.jaap.2004.12.004.

[22] I. Ziegler, R. Fournet, P. Marquaire, Pyrolysis of propane for {CVI} of pyrocarbon: Part i. experimental and modeling study of the formation of toluene and aliphatic species, Journal of Analytical and Applied Pyrolysis 73 (2005) 212 – 230. doi:doi:10.1016/j.jaap.2004.12.005.

[23] I. Ziegler, R. Fournet, P.-M. Marquaire, Pyrolysis of propane for {CVI} of pyrocarbon: Part ii. experimental and modeling study of polyaromatic species, Journal of Analytical and Applied Pyrolysis 73 (2005) 231 – 247. doi:doi:10.1016/j.jaap.2005.03.007.

[24] P. M. M. I. Ziegler, R. Fournet, Detailed kinetic modeling of polycyclic aromatic hydrocarbons formation in propane pyrolysis at high temperature/low pressure, in: Proceedings of the European Combustion Meeting 2005, 2005.

[25] I. Ziegler-Devin, R. Fournet, P.-M. Marquaire, Pyrolysis of propane for {CVI} of pyrocarbon: Part iii: Experimental and modeling study of the formation of pyrocarbon, Journal of Analytical and Applied Pyrolysis 79 (2007) 268 – 277. doi:doi:10.1016/j.jaap.2006.10.004, {PYROLYSIS} 2006: Papers presented at the 17th International Symposium on Analytical and Applied Pyrolysis, Budapest, Hungary, 22-26 May 2006.

[26] I. Ziegler-Devin, R. Fournet, R. Lacroix, P. Marquaire, Pyroly-

sis of propane for {CVI} of pyrocarbon. part iv: Main pathways involved in pyrocarbon deposit, Journal of Analytical and Applied Pyrolysis 104 (2013) 48 – 58. doi:doi:10.1016/j.jaap.2013.09.010.

[27] K. Norinaga, O. Deutschmann, K. J. Hüttinger, Analysis of gas phase compounds in chemical vapor deposition of carbon from light hydrocarbons, Carbon 44 (2006) 1790–1800.

[28] K. Norinaga, O. Deutschmann, Detailed kinetic modeling of gas-phase reactions in the chemical vapor deposition of carbon from light hydrocarbons, Industrial and Engineering Chemistry Research 46 (2007) 3547–3557.

[29] K. Norinaga, V. M. Janardhanan, O. Deutschmann, Detailed chemical kinetic modeling of pyrolysis of ethylene, acetylene, and propylene at 1073-1373 k with a plug-flow reactor model, International Journal of Chemical Kinetics (2007).

[30] N. Sánchez, A. Callejas, A. Millera, R. Bilbao, M. Alzueta, Formation of {PAH} and soot during acetylene pyrolysis at different gas residence times and reaction temperatures, Energy 43 (2012) 30 – 36. doi:doi:10.1016/j.energy.2011.12.009, 2nd International Meeting on Cleaner Combustion (CM0901-Detailed Chemical Models for Cleaner Combustion).

[31] N. E. Sánchez, Ángela Millera, R. Bilbao, M. U. Alzueta, Polycyclic aromatic hydrocarbons (pah), soot and light gases formed in the pyrolysis of acetylene at different temperatures: Effect of fuel concentration, Journal of Analytical and Applied Pyrolysis 103 (2013) 126 – 133. doi:doi:10.1016/j.jaap.2012.10.027, pyrolysis 2012.

[32] T. Bensabath, H. Monnier, P.-A. Glaude, Detailed kinetic modeling of the formation of toxic polycyclic aromatic hydrocarbons (pahs) coming from pyrolysis in low-pressure gas carburizing conditions, Journal of Analytical and Applied Pyrolysis 122 (2016) 342 – 354. doi:doi:http://dx.doi.org/10.1016/j.jaap.2016.09.007.

[33] T. N. Zwietering, The degree of mixing in continuous flow systems, Chemical Engineering Science 11 (1959) 1–15.

[34] H. S. Fogler, Elements of Chemical Reaction Engineering, Prentice Hall International Series in Physical and Chemical Engineering Sciences, 1999.

[35] D. G. Goodwin, H. K. Moffat, R. L. Speth, Cantera: An object-oriented software toolkit for chemical kinetics, thermodynamics, and transport processes, `http://www.cantera.org`, 2014. Version 2.1.2.

[36] A. Hagberg, D. Schult, P. Swart, NetworkX Refere, 2016.

[37] T. Lu, C. K. Law, Linear time reduction of large kinetic mechanisms with directed relation graph: n-heptane and iso-octane, Combustion and Flame 144 (2006) 24 – 36. doi:doi:10.1016/j.combustflame.2005.02.015.

[38] T. Lu, C. K. Law, On the applicability of directed relation graphs to the reduction of reaction mechanisms, Combustion and Flame 146 (2006) 472 – 483. doi:doi:10.1016/j.combustflame.2006.04.017.

[39] P. Pepiot-Desjardins, H. Pitsch, An efficient error-propagation-based reduction method for large chemical kinetic mechanisms, Combustion and Flame 154 (2008) 67 – 81. doi:doi:10.1016/j.combustflame.2007.10.020.

[40] T. M. K. Coles, Model Simplification of Chemical Kinetics Systems Under Uncertainty, Master's thesis, Massachusetts Institute of Technology, 2011.

[41] S. H. Lam, Using csp to understand complex chemical kinetics, Combustion Science and Technology 89 (1993) 375–404. doi:doi:10.1080/00102209308924120.

[42] S. H. Lam, D. Goussis, The csp method for simplifying kinetics, International Journal of Chemical Kinetics 26 (1994) 461–486.

[43] J. M. Ortega, H. N. Najm, J. Ray, M. Valorani, D. A. Goussis, M. Frenklach, Adaptive chemistry computations of reacting flow, Journal of Physics: Conference Series 78 (2007) 012054.

[44] L. Liang, K. Puduppakkam, E. Meeks, Towards using realistic chemical kinetics in multidimensional cfd, Nineteenth International Multidimensional Engine Modeling User's Group Meeting (2009).

[45] N. J. Curtis, K. E. Niemeyer, C.-J. Sung, An automated target species selection method for dynamic adaptive chemistry simulations, Combustion and Flame 162 (2015) 1358 – 1374. doi:doi:10.1016/j.combustflame.2014.11.004.

[46] J. Tóth, A. L. Nagy, I. G. Zsély, Structural analysis of combustion mechanisms, Journal of Mathematical Chemistry 53 (2015) 86–110. doi:doi:10.1007/s10910-014-0412-3.

[47] A. C. Hindmarsh, P. N. Brown, K. E. Grant, S. L. Lee, R. Serban, D. E. Shumaker, C. S. Woodward, SUNDIALS: Suite of nonlinear and differential/algebraic equation solvers, ACM Transactions on Mathematical Software 31 (2005) 363–396.

[48] H. G. Weller, G. Tabor, H. Jasak, C. Fureby, A tensorial approach to computational continuum mechanics using object-oriented techniques, Computers in Physics 12 (1998) 620–631. doi:doi:10.1063/1.168744.